Analysis of rainfall-induced slope failures

G. M. Rotisciani & A. Desideri
Dipartimento di Ingegneria Strutturale e Geotecnica, Sapienza Università di Roma, Roma, Italia.

F. Casini
Dipartimento di Ingegneria Civile e Ingegneria Informatica, Università degli Studi di Roma "Tor Vergata", Roma, Italia.

ABSTRACT: The hydro-mechanical behaviour of a pyroclastic soil layer covering a steep slope has been numerically investigated by performing plane strain analyses using a finite element code. The mechanical behaviour of the volcanic soil has been simulated by means of an elastic-plastic constitutive model extended to unsaturated conditions. The influence of the geometry and soil properties on the slope response has been studied by modifying the slope angle, the permeability law and the water retention curve of the pyroclastic cover. A comprehensive analysis of the slope response during the pre-failure phase is presented focusing attention on the evolution of the more significant hydro-mechanical variables and the displacement fields.

1 INTRODUCTION

Over the last few decades, several catastrophic events have been occurred in Italy, especially in Campania region i.e., Sarno (1998), Cervinara (1999), Nocera (2005). These phenomena involve essentially pyroclastic soils in the regime of partial saturation covering steep slopes. They are characterized by rapid and unexpected activation and are capable of mobilizing large volumes of material causing massive economic damages and loses of human life (Chu et. al. 2003; Olivares & Picarelli 2003; Picarelli et al. 2008).

The stability of these slopes is usually assured by the matric suction that increases soil shear strength. Intense and prolonged precipitations can appreciably modify the saturation degree in the pyroclastic cover and reduce the suction. This entails the attainment of failure conditions at the base of the unsaturated cover and consequently, the triggering of shallow landslides. These phenomena can evolve into slides or flow-slides depending on several factors including slope angle, initial conditions and soil properties. The evaluation of the suction value at which soil movements take place and the comprehension of when slope failures evolve in flow-slides are still open-issues. A deep understanding of the triggering and propagation mechanisms is required to address these questions.

This paper presents a preliminary study about the hydro-mechanical effects of the rainfall infiltration in a pyroclastic soil layer covering a steep slope. A comprehensive analysis of the slope response during the pre-failure phase is presented, focusing attention on the evolution of the more significant hydro-mechanical variables and the displacement fields.

The paper is organized as follows. In the first part, the numerical model is described together with the constitutive laws adopted for the fluid and solid phases. In the second part, the results of a parametric study are presented to point out the influence of the geometry and the hydraulic properties of the volcanic soil (permeability law and water retention curve) on the slope response.

2 FINITE ELEMENT MODEL

2.1 *Geometry, boundary and initial conditions*

The hydro-mechanical response of a pyroclastic soil layer covering a steep slope has been investigated by performing several plane strain numerical analyses. The thickness of the pyroclastic cover is 2.0 m and, the slope angle is 30°.

The soil domain has been discretized by a finite element mesh of 30 m along ξ direction and 2.4 m in η direction, with element size varying from (0.2 m x 0.1 m) in the pyroclastic cover to (0.2 m x 0.2 m) in the base layer. The finite element mesh adopted in this study is drawn in Figure 1 together with the reference system (ξ, η). The ξ axis is assumed to be parallel to the slope surface and the η axis is directed normally to the upper boundary. As demonstrated by several preliminary analyses, the mesh shown in Figure 1 returns stable and accurate solutions, which do not appreciably change reducing zone dimensions.

The nodes at the lower boundary are constrained by hinges while the nodes located along the lateral sides of the base layer can move normally to the soil surface.

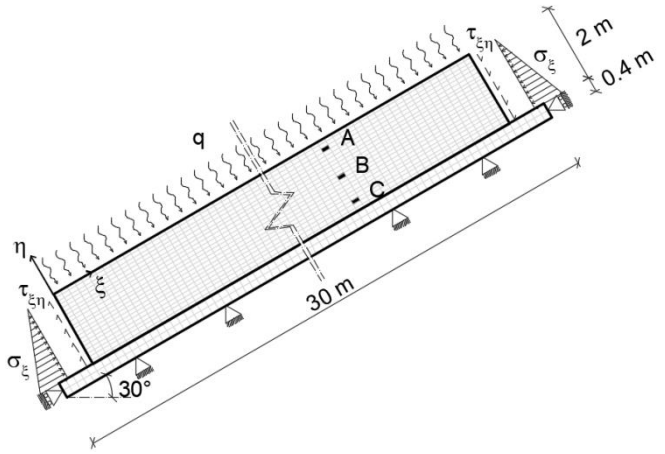

Figure 1. Finite element mesh.

Normal and shear stresses increasing with depth are applied on the lateral sides of the pyroclastic cover. The stress distributions are calculated considering the soil domain as an infinite unsaturated slope. Water flux is prevented at the lower boundary; no flux is allowed through the lateral sides until when the soil is in partially saturation regime.

The interaction between the pyroclastic cover and the base layer is modelled as a purely frictional contact with Mohr Coulomb failure criterion.

Under geostatic conditions, the total normal σ_η and shear $\tau_{\xi\eta}$ stresses acting on planes parallel to the upper surface increase with depth reaching values of 29 and 17 kPa at the base of the pyroclastic soil, respectively. The effective normal stresses σ_ξ' acting on planes perpendicular to the soil surface are calculated assuming a factor C equal to 1. This implies that σ_ξ' coincides with σ_η'. The water table is initially located at a depth of 2.5 m from the upper boundary. The pore water pressures vary linearly with depth from -21.6 kPa at the soil surface to -4.3 kPa at the base of the pyroclastic cover.

Starting from the initial conditions, a constant water flux is prescribed at the upper boundary. The flux is directed normally to the soil surface and its magnitude coincides with the saturated permeability of the soil, k_{sat}. The corresponding water inflow varies in time according to the current values of saturation degree and hydraulic gradient.

2.2 *Constitutive laws*

The mechanical behaviour of the volcanic soil is described using the Modified Cam Clay Model, MCCM, extended to partially saturated conditions following the approach proposed by Jommi and Di Prisco (1994). The mathematical formulation of this model is described in detail in Tamagnini (2004) and Rotisciani et al. (2015). Here, only the main characteristics are reported. The MCCM is formulated within the framework of critical state soil mechanics in terms of Bishop's effective stresses. The latter are defined as: $\sigma'_{ij} = \sigma_{ij} + \chi\, s\, \delta_{ij}$; where σ_{ij} is the total stress; χ coincides with the saturation degree S_r; s is the suction and δ_{ij} is the Kronecker delta.

In this model the yield surface is an ellipse centered on the p' axis:

$$F := q^2 - M^2 p'\left(p_c' - p'\right) \tag{1}$$

where, p_c' is the pre-consolidation pressure and M defines the slope of the critical state line in the stress invariant plane (p', q).

Inside the yield surface, the model predicts an isotropic hypo-elastic response. The evolution laws of the elastic moduli are deduced from the unloading-reloading line (URL) assuming a constant value for Poisson's ratio ν. The flow rule is assumed to be associated and the evolution of the yield surface results from a double-hardening mechanism:

$$\dot{p}_c' = \frac{v p_c'}{\lambda - \kappa}\dot{\varepsilon}_v^p - b p_c' \dot{S}_r \tag{2}$$

where, v is the specific volume; λ and κ are the slopes of the Normal Consolidation Line (NCL) and the URL in a semi-logarithmic picture of the compressibility plane; b is a constitutive parameter which controls the relative position of the NCL associated with the current saturation degree with respect to the saturated NCL. The mechanical effects of changing in S_r are considered with the explicit dependence of p_c' from S_r, i.e., the collapse upon wetting (Casini 2012) and the changes in the pre-consolidation stress (Casini et al. 2013).

The fluid flow is described by the well-known Richards equation:

$$\nabla\left(\frac{k}{\gamma_w}\nabla\left(s + \gamma_w z\right)\right) = \frac{\partial\left(n S_r\right)}{\partial t} \tag{3}$$

where, γ_w is the specific weight of water; z is the depth; n is the porosity and, k is the unsaturated permeability defined as: $k = k_{sat}\, k(S_r)$, where $k(S_r)$ obeys the Van Genuchten expression (Fig. 2):

$$k\left(S_r\right) = \sqrt{S_r}\cdot\left[1 - \left(1 - S_r^{\,\delta}\right)^{\beta}\right]^n \tag{4}$$

in which, δ, β and n are three constitutive parameters to calibrate on the basis of experimental data.

The Water Retention Curve (WRC) defines the relationship between the suction and saturation degree. In this study, a Van Genuchten type WRC has been adopted (see Fig. 3):

$$S_r = S_{r,res} + \left(1 - S_{r,res}\right)\Big/\left(1 + \left(\alpha s\right)^n\right)^m \tag{5}$$

where $S_{r,res}$ is the residual saturation degree and the parameters α, n and m control the shape of the curve. The experimental data point out a reversible

behaviour along drying/wetting paths and negligible effects of soil deformation on the retention curve.

The MCCM, the permeability curve and the WRC are calibrated against the results of laboratory tests carried out on undisturbed soil samples taken from Cervinara. The calibration procedures are described in Rotisciani et al. (2015); the values adopted for the parameters are listed in Table 1.

The base layer is modelled as a linear elastic material with high stiffness moduli and hydraulic permeability two orders of magnitude lower than that of pyroclastic cover.

The predictive capabilities of the MCCM have been evaluated in several studies with reference to single elements (Tamagnini 2004; Casini 2012; Casini et al. 2013) and in real problems, as for example, the evaluation of wetting-induced settlements in horizontal soil layers (Rotisciani et al. 2014) and in road embankments (Rotisciani et al. 2017).

Tab. 1. Mechanical and hydraulic parameters.

MCCM			WRC			$k(S_r)$	
			WRC_1	WRC_2		$k(S_r)_1$	$k(S_r)_2$
λ	0.22	α	0.13	0.08	δ	6	0.138
κ	0.03	m	0.57	0.49	β	2.5	$2\ 10^{-4}$
ν	0.25	n	2.32	1.96	n	1.5	0.55
M	1.45	S_{res}	0.36	0.41	k_{sat}	$1.4\ 10^{6}$	$1.4\ 10^{6}$
N	3.78				(m/s)		
b	5.0						

2.3 *Parametric study*

Five numerical analyses have been carried out modifying the slope angle α, the permeability law $k(S_r)$ and the WRC, as summarized in Table 2. The parametric study aims to investigate to what extent the geometry and hydraulic properties influence the hydro-mechanical behaviour of the unsaturated infinite slope. Emphasis is given to the analysis of the time evolution of the infiltration process and the wetting-induced displacement field.

The slope angle ranges from 25° to 37°, the last value is greater than the critical friction angle of the cover. The permeability curves adopted in this study are depicted in Figure 2: $k(S_r)_1$ shows a gradual reduction of soil permeability with S_r; $k(S_r)_2$ points out a sharp reduction of k passing from saturated to unsaturated regime. The WRCs are drawn in Figure 3. They differ in the air-entry value, the $S_{r,res}$ and the slope of the curve for suction levels lower than 15 kPa. The curves $k(S_r)_2$ and WRC_2 refer to a fine-grained soil with quite different characteristics from the volcanic ashes (Rotisciani et al. 2015).

3 NUMERICAL RESULTS

The results of the reference test T1 are described in detail emphasizing the main aspects of the hydro-mechanical response of the slope in the pre-failure phase.

Table 2. Summary of numerical analyses.

Test	α (°)	$k(S_r)$	*WRC*
1	**30**	$\boldsymbol{k(S_r)_1}$	$\mathbf{WRC_1}$
2	25	$k(S_r)_1$	WRC_1
3	37	$k(S_r)_1$	WRC_1
4	30	$k(S_r)_2$	WRC_1
5	30	$k(S_r)_1$	WRC_2

Note: Bold identifies the reference analysis.

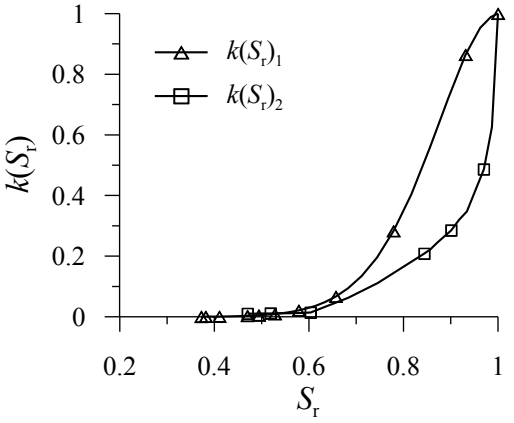

Figure 2. Permeability laws.

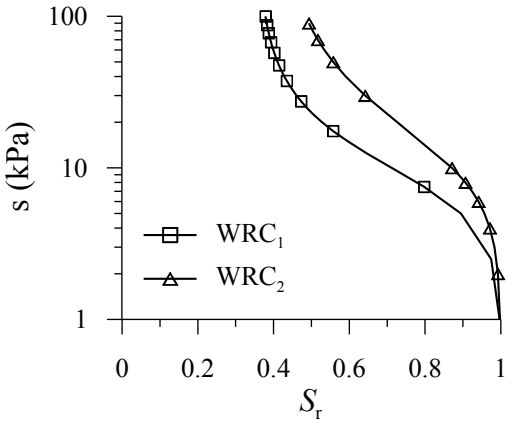

Figure 3. Water retention curves.

Figure 4 shows the time evolution of S_r profiles along a normal axis to the slope surface. When the water flux is prescribed at the upper boundary, a wetting front starts to move downwards through the pyroclastic cover. As the front deepens, the saturation degree increases approaching values close to the unity. However, full saturation is achieved only when the wetting front reaches the bottom of the pyroclastic cover and a saturation front starts to move upwards through the layer. Similar results were obtained analysing the time evolution of the imbibition process in a horizontal homogeneous soil layer (Rotisciani et al. 2015). During the rising of the water table, failure conditions are achieved at the base of the pyroclastic layer. The upper part of the soil layer remains in partially saturation regime. In this case, the failure mechanism evolves as a slide along the contact surface between the pyroclastic cover and the stiff base layer.

Time evolution of the pore-water pressure u in three elements (A, B and C) located at increasing distance from the slope surface (η=-0.25, -1.05, -1.75 m; (Fig. 1)) are depicted in Figure 5. When the front is still above the considered elements, no appreciable variation of u is observed. As soon as the wetting front passes through the selected elements, the pore water pressure quickly increases. Once the wetting front reached the base of the pyroclastic soil, the saturation front starts to rise to the slope surface. This entails the attainment of positive pore water pressures in the deep element and a further increase of u in the element B. Contrary, no additional variation of u is observed in the element A: this means that the failure occurs before the saturation front passes, rising from the base, through the shallow element.

In this simulation, the triggering of the shallow landslide is due to the increase of the pore-water pressure at the base of the unsaturated cover. This increase causes a reduction of σ_η' acting on the contact surface between the cover and the base layer and, consequently, a reduction of the maximum shear stress that can be mobilized along this surface. When the latter becomes lower than $\tau_{\xi\eta}$, the cover starts to slide on the base layer. Therefore, the instability mechanism is a classical shear failure.

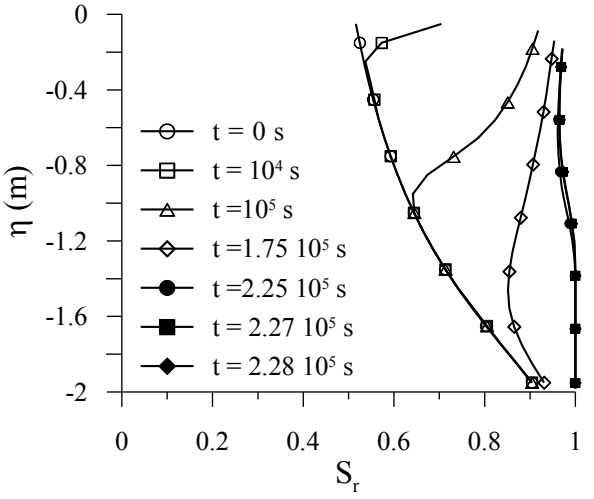

Figure 4. Isochrones of S_r for the T1.

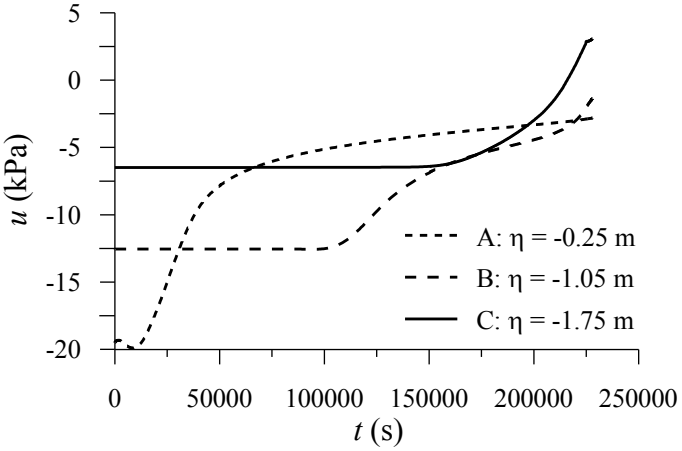

Figure 5. Time evolution of u in elements A, B, C.

The changes in time of the displacements along η and ξ directions, δ_η and δ_ξ, are reported in Figure 6 with reference to three nodes located at the upper boundary P_1, in the middle of the soil layer P_2 and at the bottom of the cover P_3. When the wetting front propagates within the soil layer, the saturation degree increases as well as the pore-water pressure. Despite the mean effective stress decreases, solid skeleton collapses causing irreversible positive volumetric strains and consequently, significant settlements at the slope surface (P_1 in Fig. 6). Further settlements occur when the saturation front rises through the soil layer even if they develop slower than those observed in the first part. Time evolution of δ_η in the node P_2 is quite different from that just described. No significant displacement is registered as long as the wetting front moves above the considered node. The settlements start to develop when the wetting front moves below the middle of the soil layer and stop when the saturation front, moving from the bottom, reaches the considered node. Finally, no appreciable displacement along η direction is registered in the node P_3, as expected due to the high stiffness of the base layer.

The displacements along ξ direction, are mainly due to the progressive accumulation of the distortional strains in soil elements during the imbibition process. Time evolution of δ_ξ is qualitatively similar to that of δ_η (Fig. 6). Indeed, δ_ξ increases in magnitude as the soil layer is wetted reaching the maximum value at the upper boundary and keeping null value at the base. The abrupt increase of δ_ξ indicates the attainment of failure conditions.

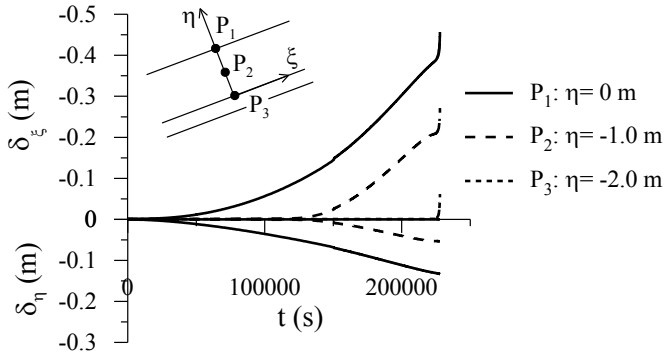

Figure 6. Time evolution of δ_ξ and δ_η.

3.1 *Influence of the slope angle*

In order to investigate the influence of the geometry on the slope behaviour, three numerical analyses have been conducted with the angle α ranging between 25° and 37°.

The initial conditions, in terms of stress state, suction level and saturation degree, are substantially coincident: the small differences derive from the changes in model geometry. Regardless of the values for α, the evolutions in time of S_r and u are qualitatively similar to those depicted in Figures 4 and 5. The slope angle has a little influence on the time

evolution of δ_η and δ_ξ: the displacements develop earlier and faster when the inclination angle is greater. However, the main difference in the tests T1, T2 and T3 concerns when the landslide occurs. As widely expected, the failure conditions are achieved more quickly as the slope angle increases.

Figure 7 shows the final values of the pore-water pressure in the elements A, B and C located at increasing distance from the slope surface. When the slope angle is equal to 25°, positive pore-water pressures are registered in all considered elements with increments ranging from 17 kPa (in the deep element) to 22 kPa (in the shallow element). In the reference test T1, full saturation is reached only in the lower part of the soil layer. In this case, the reduction of the suction level that causes the failure mechanism is about 8 kPa. In the Test T3, the slope stability is completely assured by the suction level: as soon as it decreases (1 kPa), the instability phenomenon occurs. In this case, the failure conditions are achieved when the soil layer is still in unsaturated regime.

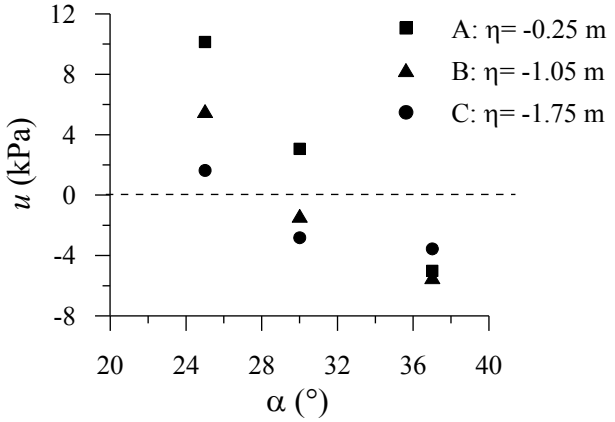

Figure 7. Influence of α on the pore-water pressures at failure.

3.2 *Influence of the hydraulic properties*

The influence of the soil hydraulic properties on the slope response has been investigated by comparing the results of the tests T1, T4 and T5. The T1 and T4 differ only in the expression of the permeability law (Fig. 2) while the T1 and T5 in the shape of WRC (Fig. 3), as reported in Table 2.

Figure 8 shows the isochrones of S_r along a normal axis to the slope surface for the T4. Like the T1, when the water flux is imposed at the upper boundary, a wetting front starts to move through the soil layer. The S_r profiles point out a slower and less diffuse front propagation than that observed in the T1. Moreover, the abrupt reduction in k for S_r <1.0 prevents the water to quickly infiltrate through the soil layer and entails the attainment of full saturation above the current position of the wetting front.

Coherently to the S_r evolution, when the wetting front passes through a soil element, the pore water pressure increases approaching a null value. The pore-water pressure keeps a quite constant value until the water table moves upwards from the bottom and reaches to the considered element. As soon as u at the base of soil layer is about 4 kPa, the pyroclastic cover starts to slide. It is to be noted that, the variation of u that causes the triggering of the shear failure coincides with that observed in T1, even if globally the spatial distribution of u is different in two analysed cases.

Finally, modifying the shape of the permeability law, no appreciable difference has been found in the final values of the displacements δ_ξ and δ_η.

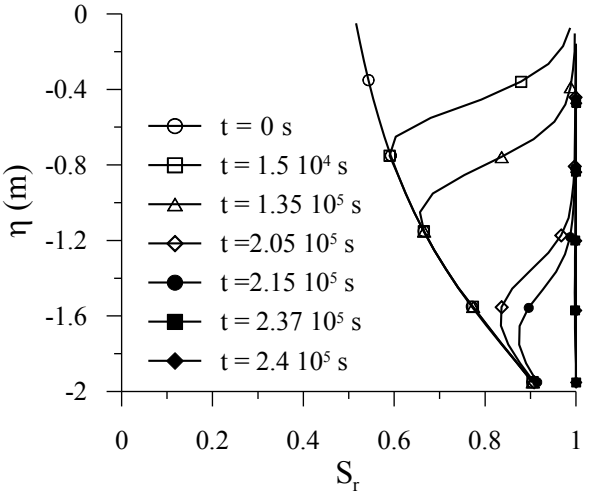

Figure 8. Isochrones of S_r for the T4.

Considering the tests T1 and T5, Figure 9 shows the isochrones of S_r for the T5 along a normal axis to the slope surface. Comparing these results with those shown in Figure 4:

- the initial distribution of S_r is different in the two analysed cases. Keeping the initial position of the water table unchanged, at a given depth, S_r is greater in the T5 than in T1. Obviously, this depends on the WRC adopted in the simulation;
- the wetting front is more diffused and propagates more quickly in the T5 than in the T1. At a given time, the saturation level and consequently, the soil permeability is higher when WRC_2 is adopted;
- in both cases, the infiltration process can be divided in two parts: the propagation of the wetting front from the upper boundary to the bottom; the rising of the saturation front form the base to the top.

The shape of WRC influences the time evolution of the pore-water pressure but has no effect on its final value. The increase of u that triggers the slope failure is substantially coincident in the T1 and T5 and is about 4 kPa.

Contrary to what was observed for u, the change in the WRC markedly affects the wetting-induced displacements. In both cases, as S_r increases, the solid skeleton collapses causing irreversible volumetric and distortional strains. The magnitude of the plastic strains generally depends on: the tendency of the soil to collapse upon wetting, the initial conditions in terms of S_r, the variation of S_r. In all tests the param-

eter b, that controls the changes in volume of the yield surface due to the variations of S_r, is equal to 5. This means that, the material behaves as a collapsing soil in both cases. Conversely, there are some differences in the initial values for S_r and in the final increments of saturation level. At a given depth, S_r is greater in the T5 than in T1 and consequently, the variation of S_r is lower when WRC_2 is adopted. This implies that, the magnitude of the wetting-induced displacements in the T5 are significantly lower than those occurred in the T1 (about one third).

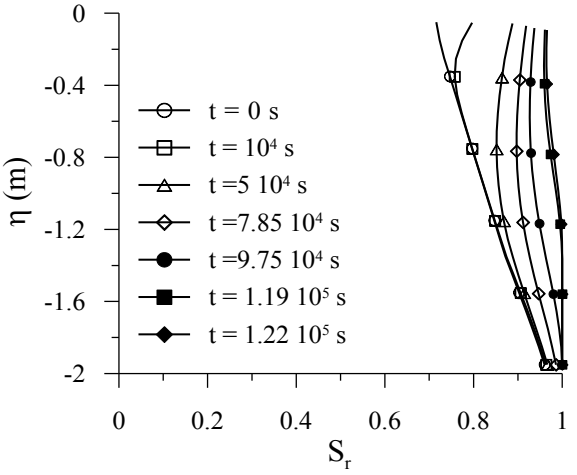

Figure 9. Isochrones of S_r for the T5.

4 CONCLUDING REMARKS

The numerical study aims to investigate to what extent the geometry and the hydraulic properties influence the response of a pyroclastic soil layer covering a steep slope. The hydro-mechanical behaviour of the volcanic ash has been modelled using the Modified Cam Clay model extended to unsaturated conditions. The constitutive model has been calibrated against the results of laboratory tests carried out on soil samples taken from the site of Cervinara. Here, over the last decades several rainfall-induced landslides have been occurred causing damages in pre-existing buildings and loses of human life.

Based on the numerical results, the following conclusions are drawn:

- the slope angle controls the amount of the suction removal that causes the triggering of the instability phenomenon. If α is greater than the critical friction angle, failure conditions are achieved when the pyroclastic cover is still in unsaturated regime;
- the permeability law mainly affects the evolution in time of the infiltration process. Assuming a soil permeability that gradually varies with S_r, when slope failure occurs, complete saturation is attained only in the lower part of the pyroclastic cover (η <-1.35 m). Conversely, assuming a sharp reduction of k as soon as S_r drops below the unity, the landslide involves a fully saturated soil layer;
- the WRC modifies the time evolution of the imbibition process and the wetting-induced displacement field. Keeping the initial distribution of u unchanged, the shape of WRC controls the initial values for S_r and consequently, the final variation of saturation level.

The predictions of flume tests carried out on volcanic ashes taken from Cervinara (Bogaard et al. 2014) are ongoing. The numerical results will be compared with the measurements to verify the ability of the constitutive model to correctly reproduce the slope response in the pre-failure phase. Preliminary results show that the model satisfactorily describes time evolution of S_r and u and tends to underestimate the wetting-induced deformations.

Finally, in all analysed cases, the slope failure evolves into slide along the base of the pyroclastic cover. These likely results from the constitutive model adopted in the presented study. Therefore, we are planning to use a constitutive model with not-associated flow rule in order to capture landslides evolving into flow-slides in the following analyses.

5 REFERENCES

Bogaard, T.A., Greco, R., Olivares, L. & Picarelli, L. 2014. The Round Robin test on landslide hydrological modelling at IWL 2013. *Procedia Earth and Planetary Science* 9: 180-188.

Casini, F. 2012. Deformation induced by wetting: a simple model. *Canadian Geotechnical Journal* 49(8): 954–960.

Casini, F., Serri, V. & Springman, S.M. 2013. Hydromechanical behaviour of a silty sand from a steep slope triggered by artificial rainfall: from unsaturated to saturated conditions. *Canadian Geotechnical Journal* 50(1): 28–40.

Chu, J., Leroueil, S. & Leong, W.K. 2003. Unstable behaviour of sands and its implications for slope instability. *Canadian Geotechnical Journal* 40(5): 873–885.

Jommi, C. & di Prisco, C. 1994. A simple theoretical approach for modelling the mechanical behaviour of unsaturated soils. *In Italian Conference, Il ruolo dei fluidi nei problemi di ingegneria geotecnica*, Mondovi: 167–188.

Olivares, L. & Picarelli, L. 2003. Shallow flowslides triggered byintense rainfalls on natural slopes covered by loose unsaturated pyroclastic soils. *Géotechnique* 53(2): 283–287.

Picarelli, L., Olivares, L., Comegna, L. & Damiano, E. 2008. Mechanical aspects of flow-like movements in granular and fine-grained soils. R*ock Mechanics and Rock Engineering* 41(1): 179–197.

Rotisciani, G.M., Sciarra, G., Desideri, A. & Casini, F. 2014. Modeling rainfall infiltration through coarse and fine-grained unsaturated geomaterials. *Unsaturated Soils: Research & Applications*: 521-528.

Rotisciani, G.M., Sciarra, G., Casini, F. & Desideri, A. 2015. Hydro-mechanical response of collapsible soils under different infiltration events. *International Journal for Numerical and Analytical Methods in Geomechanics* 39(11): 1212–1234.

Rotisciani, G.M., Casini, F., Desideri, A. & Sciarra, G. 2017. Hydromechanical behavior of an embankment during inundation. *Canadian Geotechnical Journal* 54(3): 348-358.

Tamagnini, R. 2004. An extended Cam-clay model for unsaturated soils with hydraulic hysteresis. *Géotechnique* 54(3): 223–228.